


Impact of network topology on self-organized criticality

Heiko Hoffmann*

HRL Laboratories, LLC, Malibu, California 90265, USA
 (Received 31 October 2017; revised manuscript received 3 January 2018; published 22 February 2018)

The general mechanisms behind self-organized criticality (SOC) are still unknown. Several microscopic and mean-field theory approaches have been suggested, but they do not explain the dependence of the exponents on the underlying network topology of the SOC system. Here, we first report the phenomena that in the Bak-Tang-Wiesenfeld (BTW) model, sites inside an avalanche area largely return to their original state after the passing of an avalanche, forming, effectively, critically arranged clusters of sites. Then, we hypothesize that SOC relies on the formation process of these clusters, and present a model of such formation. For low-dimensional networks, we show theoretically and in simulation that the exponent of the cluster-size distribution is proportional to the ratio of the fractal dimension of the cluster boundary and the dimensionality of the network. For the BTW model, in our simulations, the exponent of the avalanche-area distribution matched approximately our prediction based on this ratio for two-dimensional networks, but deviated for higher dimensions. We hypothesize a transition from cluster formation to the mean-field theory process with increasing dimensionality. This work sheds light onto the mechanisms behind SOC, particularly, the impact of the network topology.

DOI: [10.1103/PhysRevE.97.022313](https://doi.org/10.1103/PhysRevE.97.022313)

I. INTRODUCTION

Complex systems of interacting components are widespread in nature and manmade structures—see, e.g., tectonic plates and power grids. In some of those systems, scale-invariant fluctuations have been observed that occur spontaneously without the need to carefully tune a control parameter like, e.g., the temperature [1–6]. Examples of these fluctuations are earthquakes [6], avalanches in a sand pile [1], power outages [4], or avalanches of neural spikes [2]. Since these systems apparently self-organize to generate scale-invariant fluctuations, this phenomenon has been termed self-organized criticality (SOC).

Typically, SOC occurs in systems with threshold dynamics and an external driving force, e.g., the addition of new sand grains [5]. However, the precise characteristics that guarantee SOC are still unknown. The occurrence of SOC has practical implications because scale-invariant fluctuations imply power-law distributed event sizes, which means that extraordinarily large events occur orders of magnitude more likely than equally sized events from a normal distribution—important when you consider, e.g., power outages.

The most common model of SOC and the first to introduce the concept has been the Bak-Tang-Wiesenfeld (BTW) model [1], which is a cellular automaton on a lattice and a simplified version of a sandpile—see Sec. II. The avalanches from this model are power-law distributed. Bak *et al.* already showed a dependence of the exponent of the power law on the dimensionality of the lattice, but a theoretical explanation of this dependence is still missing.

One of the most common theoretical explanations of the power-law distribution in the BTW model is the mean-field

theory [5,7–10]. This theory predicts, in agreement with experiments, the slope of the power law to be 1.5 for lattices in six or more dimensions. For lower dimensions, however, particularly, <5 , the experimental results deviate from the theoretical value [10].

Here, we present a hypothesis for the mechanism of SOC and an explanation of the exponents of the BTW model in lower dimensions. After introducing the BTW model, we first report a discovery of a new property of avalanches in the model: in lower dimensions, after the passing of an avalanche, the sites or nodes in the interior of the avalanche resume their original state before the avalanche. These nodes form what we call a *critical cluster*. Next, we introduce a simplified model describing the formation process of these critical clusters. This formation process converges to yield approximately power-law distributed cluster sizes. In theory, we establish a link between the fractal dimension of the boundary of the clusters and the exponent of their size distribution. Then, we verify this link in simulation. Lastly, we evaluate the same fractal dimension for the critical clusters in the BTW model and find that we can predict the exponent of the cluster-size distribution within 3% for the two-dimensional (2D) square lattice and random geometric graph. In higher dimensions, the predictions diverge. Apparently, when increasing the dimensionality, we observe a transition between cluster formation and mean-field theory.

II. BTW MODEL

The BTW model describes the flow of sand grains on a network [1]. This model has been originally defined on square and cubic lattices, but it can be generalized to arbitrary graphs [11]. Here, we consider this generalized version, also referred to as the Abelian sandpile model.

Assume a graph of nodes i that each contain x_i amount of grains. The Abelian sandpile model consists of a slow and a

*hhoffmann@hrl.com

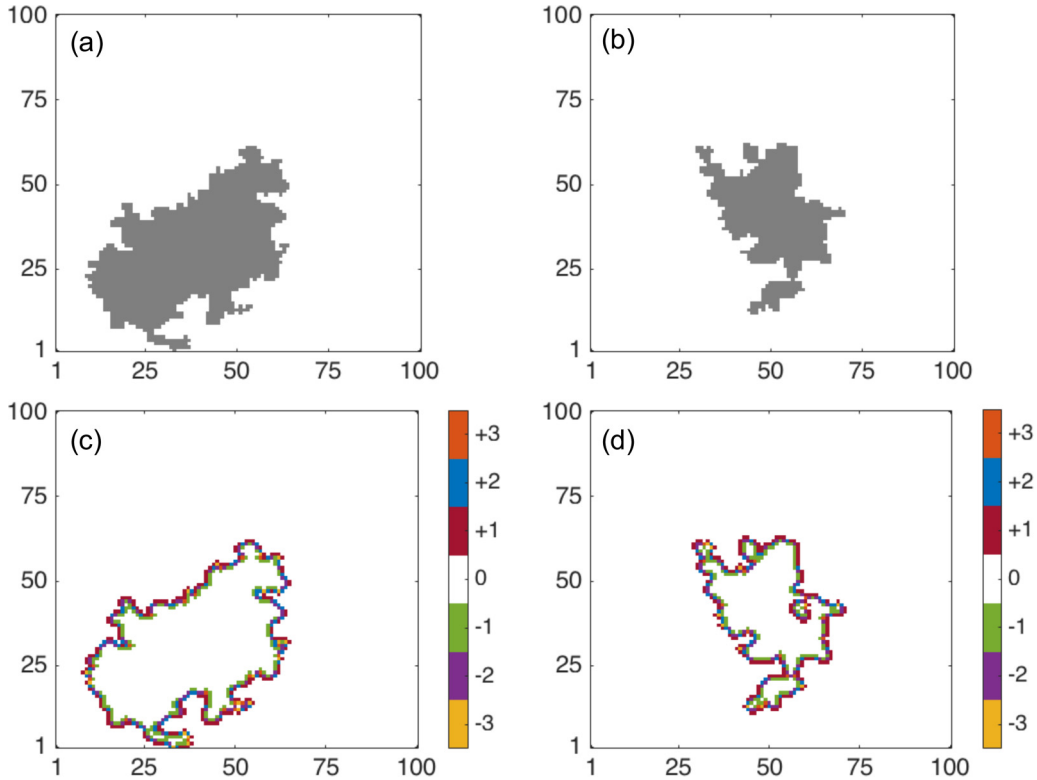


FIG. 1. BTW model leaves most of the interior of an avalanche unchanged, two typical avalanches (a) and (b) and the corresponding differences $x_i^{t+1} - x_i^t$, where x_i^t is the state of node i before and x_i^{t+1} after the avalanche, (c) and (d).

fast process. The slow process adds one grain to a random node i , $x_i \rightarrow x_i + 1$ (slow external driving force). The fast process computes the propagation of an avalanche, as described in the following. If a node is above threshold $x_i > z_i$, where z_i is the degree of node i , the node topples and sheds one grain to each of its z_i neighbors,

$$x_i(t+1) = x_i(t) - z_i, \quad (1)$$

$$\forall j \in \mathcal{N}_i : x_j(t+1) = x_j(t) + 1, \quad (2)$$

where \mathcal{N}_i is the set of nodes that share an edge with node i (here, we consider only undirected graphs). This toppling may result in a neighbor to be above threshold, making this neighbor also shed its grains according to the above equations. This repeated shedding can result in a cascade of events, an avalanche of grain topplings. Once an avalanche is complete, i.e., all nodes are at or below threshold, the slow process proceeds by adding another grain. After an initial phase of self-organization (cooling), avalanches occur with sizes that follow a power law distribution.

III. CRITICAL CLUSTERS

In the BTW model, during an avalanche, each node may topple multiple times. At the end of this process, we found that, interestingly, most nodes inside the avalanche area assume the same state as they had before the avalanche (Fig. 1). Changes to the states typically happen only at the boundary of an avalanche, while their interior reverts back to the state before the avalanche (even though all nodes inside an avalanche did topple at least once).

In a simulation of the BTW model, we computed the fraction of nodes in an avalanche that reverted back to their original state before the avalanche. We allowed for sufficient cooling time to reach SOC (see also Sec. VII). For a square lattice with side length $L = 1024$, $87.518 \pm 0.005\%$ of nodes regained their original state after one avalanche (mean \pm std, $n = 4$). This number increased with the size of the lattice because for larger clusters the boundary is smaller relative to the area. For example, for smaller lattices, we found the fraction to be $60.6 \pm 0.1\%$ for $L = 50$, $69.8 \pm 0.1\%$ for $L = 100$, and $76.6 \pm 0.3\%$ for $L = 200$.

We call the set of nodes in an avalanche that revert back to their original state a *critical cluster* because, apparently, they are carefully arranged to allow the avalanche to happen and still retain their property after the avalanche. Our critical cluster is different from a cluster of path-connected critical nodes that are just below the toppling threshold; such a cluster would also topple entirely but would change its state. Many nodes are actually near their toppling threshold. Across a 2D lattice, as part of our analysis, we observed an uneven distribution of state values, x_i , with the following probabilities: $p = 0.0738 \pm 0.0001$ for $x = 1$, $p = 0.1742 \pm 0.0002$ for $x = 2$, $p = 0.3065 \pm 0.0002$ for $x = 3$, and $p = 0.4455 \pm 0.0002$ for $x = 4$ (mean \pm std, $n = 4$); here, $L = 1024$ (see Discussion for the relevance of these numbers).

The formation of critical clusters is dependent on the dimensionality of the lattice. We simulated lattices of different dimensions with a side length $L = [1024^{2/d}]$, where d is the dimensionality. With increasing dimensionality, the fraction of unchanged nodes decreased: cubic lattice, $43.57 \pm 0.05\%$; 4D lattice, $1.967 \pm 0.007\%$; 5D lattice, $0.0112 \pm$

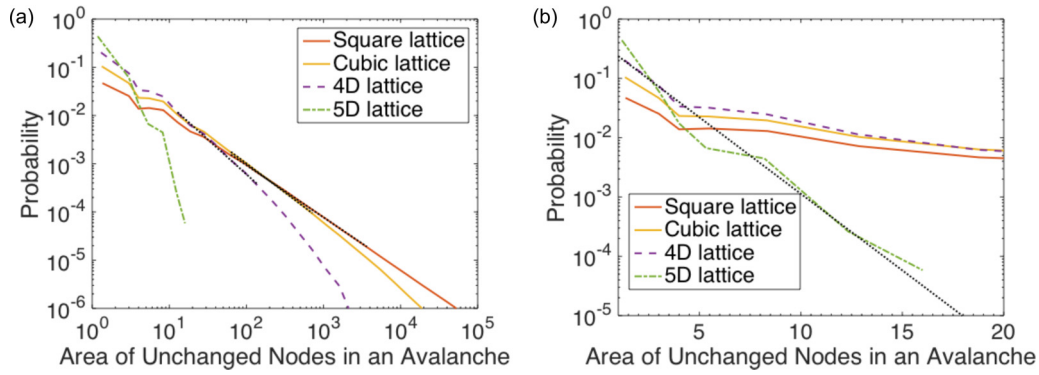


FIG. 2. Size distribution of the unchanged nodes in an avalanche is a power law (with exponential cutoff) for lattices of two, three, and four dimensions, but decays exponentially for five dimensions: log-log plot (a), dotted lines show power-law fits: semilog plot (b), dotted line shows exponential fit.

0.0001%. The fraction dropped to near zero for five dimensions. With five dimensions, the size distribution of the unchanged clusters became exponential (Fig. 2), and the probability for unchanged nodes dropped to almost zero for higher dimensions, $2 \times 10^{-5} \pm 10^{-5}\%$ for a 6D lattice, not forming any cluster of more than one node.

Due to the stability of the critical clusters, we hypothesize that they are a key element in describing the dynamic equilibrium of SOC in lower dimensions. Apparently, there exists a formation process controlling the size of these clusters. In the following, we present a simplified model of cluster formation.

IV. CLUSTER-FORMATION MODEL

The cluster-formation model describes the self-organization of a cluster-size distribution. It starts with a fixed number of clusters and then iterates merging and splitting of clusters, preserving the total number of clusters. Figure 3(a) illustrates the process in 1D. The model uses N nodes arranged along a line. These N nodes are divided into n_c connected clusters (all nodes in one cluster are path connected). In one iteration step, one node at a cluster boundary is chosen at random with uniform probability and the corresponding cluster is merged with its neighboring cluster. Given the resulting set of clusters,

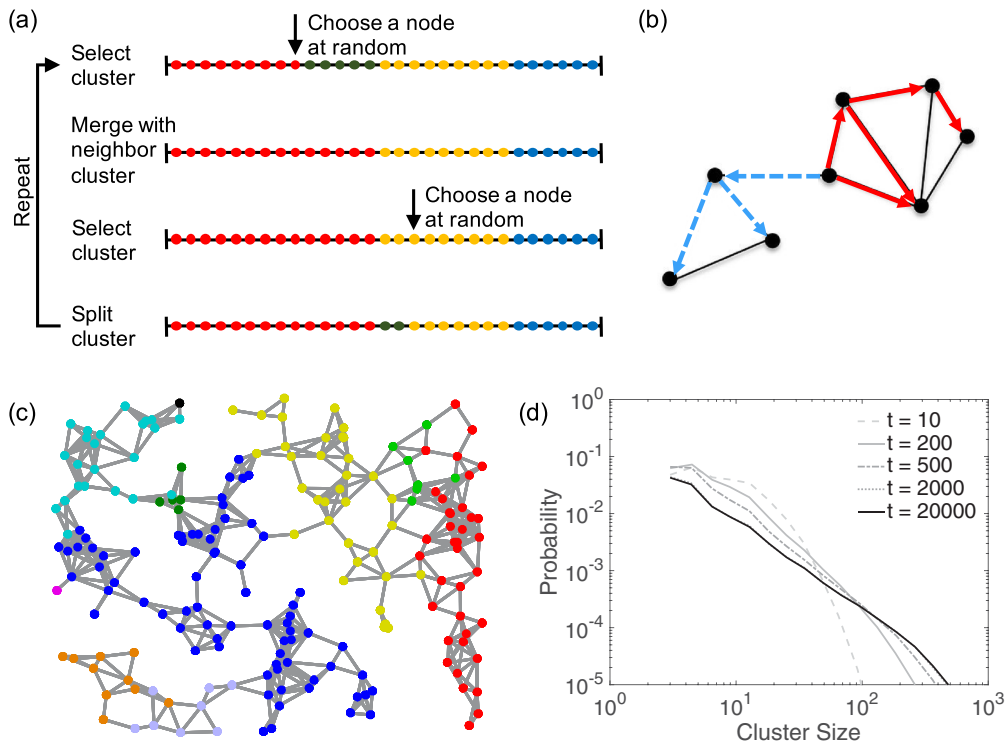


FIG. 3. Cluster formation iterates merging and splitting of clusters (a). Splitting uses two recursive breadth-first walks (solid and dashed arrows) starting from a random location (b). Iterating merge and split results in a distribution of clusters as shown, e.g., in panel (c). This iteration converges to a distribution of cluster sizes (d), here, for a cubic lattice with $N = 4096$ and $n_c = 400$ (the formation process was repeated 500 times to obtain sufficient statistics).

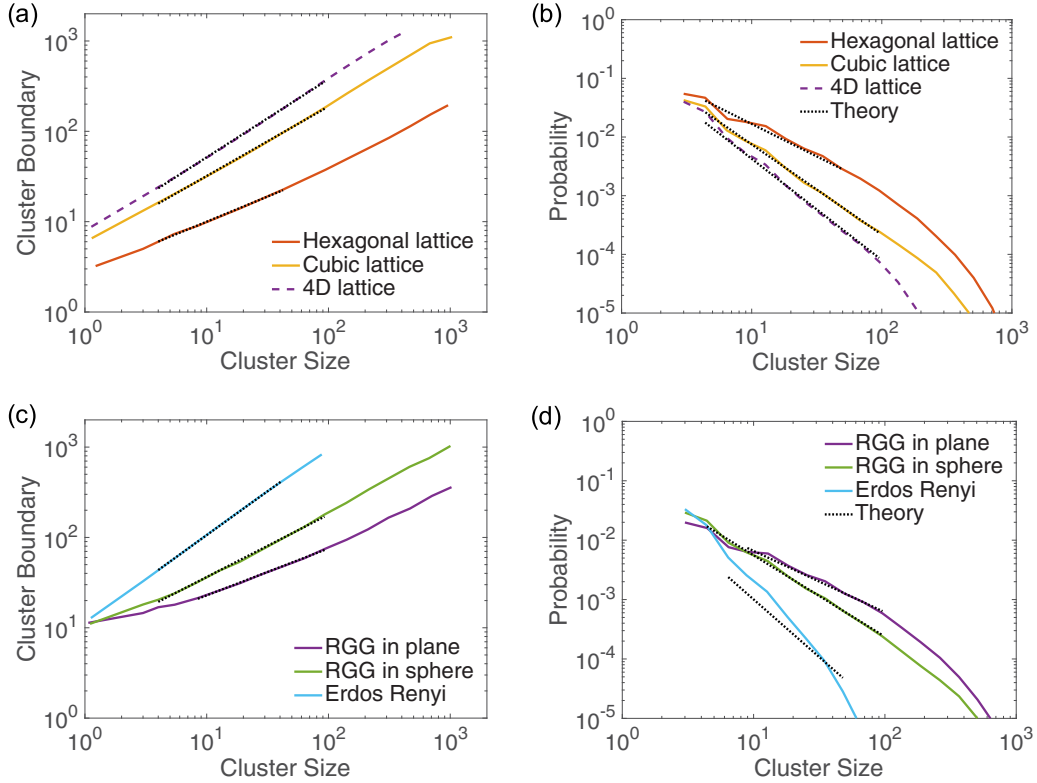


FIG. 4. Results for the cluster-formation model, showing cluster boundary versus cluster size (a), (c) and the corresponding cluster-size distribution (b), (d) for six different network types. Dotted lines in (a), (c) show power-law fits to the data and dotted lines in (b), (d) theoretical values in the same range of cluster-size values as for the power-law fits.

a new node is chosen at random with uniform probability and the corresponding cluster is split into two components at the location of the node (if a cluster with only one node is chosen, the selection is repeated).

For arbitrary graphs, we use the same merge operation as above. To split a cluster, a node from the entire graph is chosen randomly (uniform probability) such that the node has two neighboring nodes within the same cluster. These two neighboring nodes then become the starting directions for splitting the cluster. In a breadth-first search, we traverse the cluster simultaneously in two directions, splitting it into two components, e.g., solid and dashed arrows in Fig. 3(b). This process ensures that a path-connected cluster is split into two path-connected components.

To obtain the initial set of n_c clusters, we start with a single cluster and apply the above split operation until we reach n_c clusters. Then, the merging and splitting operations are repeated for a given number of iteration steps.

The split-merge iteration converges to a cluster-size distribution, which typically follows a power law for a range of cluster sizes [Fig. 3(d)]. Figure 3(c) shows a snapshot of a cluster distribution on a random geometric graph after convergence. The size distribution converges, but the clusters themselves are still dynamic.

V. THEORY OF CLUSTER FORMATION

The goal of our theoretical evaluation of the cluster-formation model is to derive a functional relationship between

the slope of the cluster-size distribution, $n(s)$, and the underlying network structure. Here, $n(s)$ is the number of clusters of size s . In the formation process, we consider the following four probabilities: the probability that a merge operation increases the number of clusters of size s , $p_m^+(s)$, the probability that a merge operation decreases this number, $p_m^-(s)$, the probability that a split operation increases this number, $p_s^+(s)$, and the probability that a split operation decreases this number, $p_s^-(s)$. At equilibrium, these probabilities need to fulfill the master equation,

$$p_m^+(s) - p_m^-(s) + p_s^+(s) - p_s^-(s) \stackrel{!}{=} 0 \quad \forall s. \quad (3)$$

For solving the master equation, our first approximation is that $p_m^+(s)$ and $p_s^-(s)$ cancel each other out, i.e., $p_m^+(s) = p_s^-(s)$. For larger cluster sizes, the appearance of a cluster due to merging dominates the appearance due to splitting and the disappearance of a cluster due to splitting dominates the disappearance due to merging: so, to balance the master equation, $p_m^+(s)$ has to compensate $p_s^-(s)$ and has to be at least approximately equal for a range of s values (in the one-dimensional case, this relationship turns out to be exact).

In the following, we consider only these two probabilities. The probability $p_s^-(s)$ is the probability that a uniformly chosen random node falls on a cluster of size s , i.e., $p_s^-(s) = \frac{n(s)s}{N}$.

The probability for merging two clusters is an integral over the combinations of cluster sizes x and $s - x$. For each of the two clusters, the probability to get selected is proportional to the boundary of the cluster because the size of the boundary

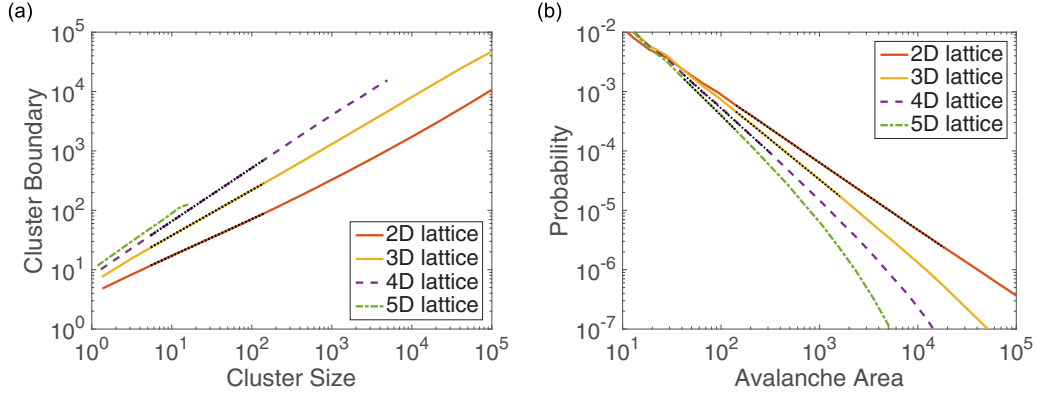


FIG. 5. BTW results: boundary of critical clusters versus their area (a) and slope of avalanche-area distribution (b); here, $L = [1024^{2/d}]$. Dotted lines show power-law functions fitted to the data.

is the number of possible merge points. So, we obtain

$$p_m^+(s) = c \sum_1^{s-1} n(x)x^\beta n(s-x)(s-x)^\beta$$

$$\approx c \int_{0.5}^{s-0.5} n(x)x^\beta n(s-x)(s-x)^\beta dx, \quad (4)$$

where c is a constant and $\beta = \frac{d_B}{d}$ with d_B the fractal dimension of the boundary and d the dimensionality of the space that the graph is embedded in. x^β is proportional to the number of surface points when x is the number of points in the volume enclosed by the surface, e.g., for a sphere $\beta = 2/3$.

For the approximate solution of the master equation, we need to solve

$$p_m^+(s) \stackrel{!}{=} p_s^-(s) = \frac{n(s)s}{N}. \quad (5)$$

Here, we use the ansatz $n(s) = as^{-\tau}$ with $\tau \geq 1$. For $p_m^+(s)$, we obtain

$$p_m^+(s) = ca^2 \int_{0.5}^{s-0.5} x^{-\tau} x^\beta (s-x)^{-\tau} (s-x)^\beta dx$$

$$= ca^2 \int_{0.5}^{s-0.5} x^{-\tau+\beta} (s-x)^{-\tau+\beta} dx. \quad (6)$$

After substituting $x = ys$, the dependence on s is more visible,

$$p_m^+(s) = ca^2 \int_{\frac{1}{2s}}^{1-\frac{1}{2s}} y^{-\tau+\beta} s^{-\tau+\beta} (s-ys)^{-\tau+\beta} s dy$$

$$= ca^2 s^{1-2\tau+2\beta} \int_{\frac{1}{2s}}^{1-\frac{1}{2s}} [y(1-y)]^{-\tau+\beta} dy. \quad (7)$$

We want to show that the last integral is approximately constant as a function of s for a reasonable range of parameters. For convenience, we set $\alpha = -\tau + \beta$, which is not positive because $\beta \leq 1$. For sufficiently large s , the values near the limits of the integral contribute the most, and we approximate

$$\int_{\frac{1}{2s}}^{1-\frac{1}{2s}} [y(1-y)]^\alpha dy$$

$$\approx \int_{\frac{1}{2s}}^{1-\frac{1}{2s}} y^\alpha + (1-y)^\alpha dy$$

$$= \frac{1}{1+\alpha} \left[\left(1 - \frac{1}{2s}\right)^{1+\alpha} - \left(\frac{1}{2s}\right)^{1+\alpha} \right]$$

$$- \left(\frac{1}{2s}\right)^{1+\alpha} + \left(1 - \frac{1}{2s}\right)^{1+\alpha}. \quad (8)$$

For sufficiently large s , the last expression can be further approximated as

$$\int_{\frac{1}{2s}}^{1-\frac{1}{2s}} [y(1-y)]^\alpha dy \approx \frac{2}{1+\alpha} [1 - (2s)^{-1-\alpha}]. \quad (9)$$

This expression is approximately constant for sufficiently large s if $\alpha > -1$. That is, we expect our analysis to hold if the slope τ of $n(s)$ is sufficiently shallow.

Given these approximations, the probability for merging is

$$p_m^+(s) \approx c' s^{1-2\tau+2\beta}, \quad (10)$$

where c' is a constant. Using this expression in the master equation (5), we obtain for the exponents

$$1 - 2\tau + 2\beta = 1 - \tau \quad (11)$$

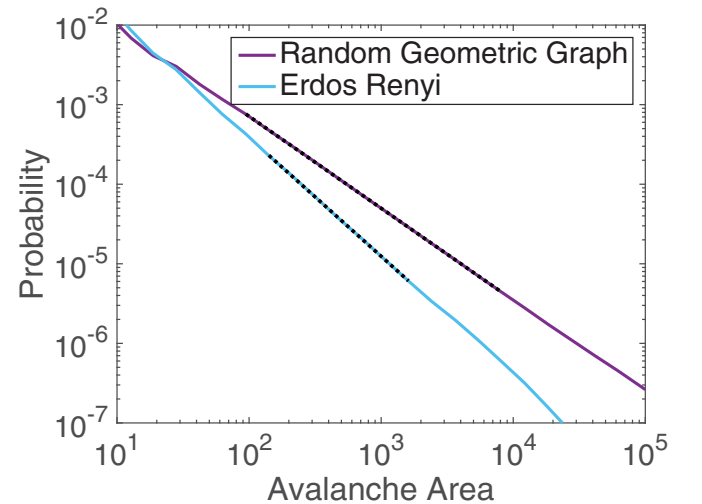


FIG. 6. Avalanche area distribution for the random geometric graph and Erdős-Renyi network; here, $N = 1024^2$. Dotted lines show power-law functions fitted to the data.

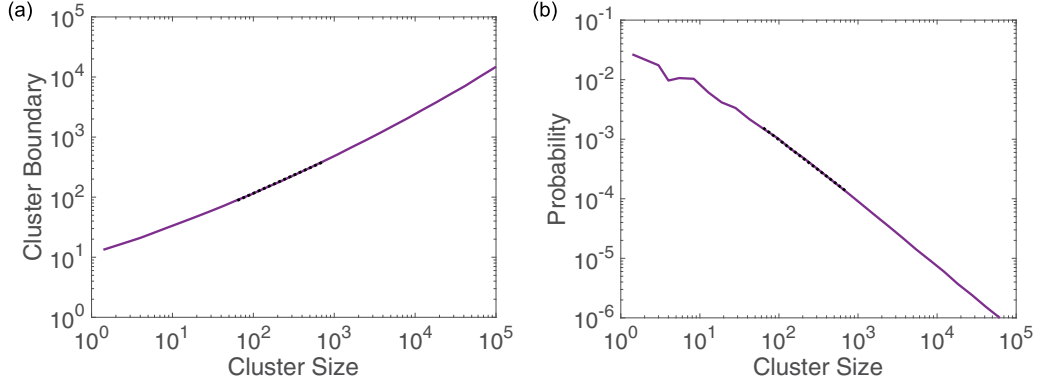


FIG. 7. BTW results on the random geometric graph: boundary of critical clusters versus their size (a) and slope of the size distribution (b); here, $N = 1024^2$. Dotted lines show power-law functions fitted to the data.

and, solving for τ , our final result

$$\tau = 2 \frac{d_B}{d}. \quad (12)$$

The slope of the cluster-size distribution is directly related to the fractal dimension of the cluster boundary. In the following, we test this relationship in simulation. The above condition $\alpha > -1$ is equivalent to $\frac{d_B}{d} < 1$. So, we expect the simulation results to differ from our theoretical approximation when the dimensionality of the boundary approaches the dimensionality of the embedding space, e.g., for Erdős-Renyí networks, $d_B = d$. For one-dimensional graphs, τ would be zero according to the above equation and our ansatz would be violated. The 1D case, however, can be solved exactly, giving $n(s) = n_c^2/N \exp(-sn_c/N)$.

The fractal dimension, d_B , is lower bounded by $d - 1$. So, τ is lower bounded by $\tau = 2 \frac{d-1}{d}$, which increases with increasing dimensionality d . That is, in higher-dimensional spaces, the exponent τ is larger and clusters tend to be smaller.

VI. CLUSTER-FORMATION RESULTS

In simulation, we evaluated the cluster-formation model and compared size distributions with the above theoretical result. We tested the relationship between slope τ and fractal dimension d_B/d on six networks: hexagonal lattice, cubic lattice, 4D lattice, random geometric graph (RGG) in a plane, RGG inside a sphere, and Erdős-Renyí (ER) network, each with $N = 4096$ nodes. The number of clusters had to be chosen carefully because it relates to the normalization constant of the power-law distribution. We chose $n_c = 200$ for the hexagonal lattice, $n_c = 400$ for the cubic one, $n_c = 1200$ for the 4D one, $n_c = 200$ for the RGG in a plane, $n_c = 400$ for the RGG in a sphere, and $n_c = 2500$ for the ER network.

For the cluster formation, we iterated the above split and merge operations 20 000 times to ensure convergence to a

cluster-size distribution. Moreover, to obtain better cluster-size statistics, this formation process was repeated 100 times, except 200 times for the hexagonal lattice (because the overall number of resulting clusters was lower) and 500 times for the ER network, which produced only a few larger clusters. For each network type, the resulting clusters were combined into one distribution, from which the fractal dimensions, d_B/d , were computed from a power-law fit to the cluster boundary versus size relationship. The overall process was repeated four times, each with a different random initialization of the random networks.

Figures 4(a) and 4(c) show one power-law fit for each network type. Across the four runs, the slopes varied only slightly: the d_B/d values for the six networks were 0.5536 ± 0.0016 for hexagonal lattice, 0.7689 ± 0.0020 for cubic lattice, 0.8627 ± 0.0003 for 4D lattice, 0.5165 ± 0.0022 for RGG in plane, 0.6850 ± 0.0057 for RGG in sphere, and 0.9710 ± 0.0007 for ER (mean \pm std, $n = 4$). Based on these values, we computed the theoretical slope, τ , according to (12). As a result, the theory matched well the simulated cluster-size distributions over the same range for which d_B/d was approximately constant (Fig. 4). As expected, our theoretical approximation deviated from the ER-network result.

VII. BTW-MODEL RESULTS

On the BTW model, we evaluated the relationship between fractal dimension and slope of the critical-cluster distribution and compared with the avalanche-area distribution. Here, the fractal dimension was computed on the boundary of the critical clusters as defined in Sec. III. We used six types of networks: 2D, 3D, 4D, and 5D lattices, RGG in plane, and ER network, each having N nodes. The lattices and the RGG had open boundaries, i.e., grains passing the boundaries of the hypercubes were lost. For ER, we used dissipation to remove

TABLE I. Fractal dimension d_B/d in the BTW model for different networks (mean \pm std, $n = 4$).

Network	RGG	2D	3D	4D
$N = 512^2$	0.6025 ± 0.0013	0.6171 ± 0.0003	0.7628 ± 0.0003	0.8919 ± 0.0010
$N = 1024^2$	0.6056 ± 0.0016	0.6177 ± 0.0003	0.7645 ± 0.0001	0.8991 ± 0.0003
$N = \infty$	0.6335 ± 0.0174	0.6233 ± 0.0035		

TABLE II. Slopes, τ_c , of critical-cluster distribution for different networks (mean \pm std, $n = 4$).

Network	RGG	2D	3D	4D
$N = 512^2$	0.978 ± 0.004	1.0609 ± 0.0006	1.219 ± 0.006	1.80 ± 0.02
$N = 1024^2$	1.010 ± 0.004	1.0835 ± 0.0006	1.224 ± 0.006	1.54 ± 0.02
$N = \infty$	1.30 ± 0.05	1.286 ± 0.007		

grains; i.e., with a small probability ($100/N$), a toppling grain did not transfer to a neighboring node and instead got removed.

We ran experiments on two network sizes, $N = 512^2$ and $N = 1024^2$, rounding the side lengths of the lattices to the nearest integer, e.g., $L = \lceil 1024^{2/3} \rceil$ for a 3D lattice. Each node was randomly initialized uniformly in the integer interval from 1 to z , where z is the toppling threshold. In each simulation run, we iterated 10 000 000 additions of one grain. For analysis, we omitted the first N iterations, allowing for sufficient cooling time to reach the SOC state. To obtain errors, experiments were repeated four times (recomputing the random graphs in each experiment).

Qualitatively, the results matched the ones for our cluster-formation model (Fig. 5). The fractal-dimension ratio d_B/d increased with dimension of the lattice, and the slope of the avalanche-area distribution also increased with increasing d_B/d . On the ER network, the avalanche-area distribution was steeper compared to the RGG (Fig. 6).

On the RGG, critical clusters formed as on the 2D square lattice. Different from the square lattice, though, the slopes of the cluster and boundary size distributions were slightly curved (Fig. 7). The slope of the probability distribution of cluster sizes curved in a way that was consistent with our cluster-formation hypothesis: the slope was steeper for sizes at which the boundary curve was steeper too. We evaluated the slope at a near straight section (dotted lines in Fig. 7), using the same cluster-size interval for both boundary and probability curves (the corresponding numerical values of the slopes are shown Tables I and II).

We evaluated the fractal dimensions d_B/d (Table I) and the exponents of the distributions for the critical-cluster size, τ_c , and the avalanche area, τ_a (Tables II and III). The fractal dimensions and critical-cluster slopes could be evaluated only for dimensions smaller than five (see Sec. III). The slopes increased with increasing dimensionality of the embedding space of the network. Across different network sizes, the fractal dimensions varied less compared to the slopes. For the 2D lattice and RGG, we also estimated slopes at infinite lattice size, as described in [12], and applied the same method for the fractal dimensions. The same extrapolation, however, does not hold for higher dimensions.

As a result, for d_B/d at $N = \infty$, according to the cluster-formation hypothesis, the expected slopes were 1.247 ± 0.007

and 1.27 ± 0.03 for the 2D lattice and RGG, respectively. In comparison, for the estimated slopes at infinity, we obtained for the 2D lattice $\tau_c = 1.286 \pm 0.007$ and $\tau_a = 1.301 \pm 0.006$ ([12] reported $\tau_a = 1.33 \pm 0.01$) and for RGG $\tau_c = 1.30 \pm 0.05$ and $\tau_a = 1.37 \pm 0.03$. These errors are only statistical and do not take into account systematic errors when extrapolating to infinity due to the uncertain dependence on N .

For the 2D networks, the estimates based on the cluster-formation hypothesis were close to the experimental values of τ_c . For the cubic and 4D lattices, the theoretically expected slopes would be larger than the mean-field value of 1.5, while they are known to be smaller [10]. So apparently, our theory deviates with increasing dimensionality, and the slopes instead approach the mean-field value—see Discussion.

VIII. DISCUSSION

We discovered a phenomenon in the BTW model for low dimensions, and based on this phenomenon suggested a mechanism behind the self-organized critical fluctuations. This mechanism approximately predicted the exponent of the avalanche-area distribution on networks embedded in two dimensions.

In low dimensions, critical clusters of nodes formed in the BTW model that enabled the propagation of an avalanche and, at the same time, remained unchanged by the passing of the avalanche. This formation is, apparently, restricted to networks embedded in two, three, or four dimensions. The critical clusters disappeared in six or more dimensions, and there was a transition between four and six dimensions. This transition coincides with the lower boundary of the dimensionality for which the mean-field theory correctly predicts the exponent of the avalanche-size distribution [10].

The mean-field theory assumes or implies that the state values of the nodes are distributed with equal probability [5]. In contrast, in our experiments, we found that this distribution is skewed towards values near the toppling threshold for lattices in lower dimensions. So, the inability of the mean-field theory to explain exponents in low dimensions is to be expected. Moreover, interestingly, the probability of a node at critical value (0.446 in our experiments with a 2D lattice) is lower than the percolation threshold (about 0.593 for site percolation in a 2D lattice [13]). So, path-connected clusters of

TABLE III. Slopes, τ_a , of avalanche-area distribution for different networks (mean \pm std, $n = 4$).

Network	RGG	2D	3D	4D	5D	ER
$N = 512^2$	1.135 ± 0.003	1.1174 ± 0.0007	1.358 ± 0.003	1.515 ± 0.007	1.673 ± 0.018	1.495 ± 0.005
$N = 1024^2$	1.159 ± 0.002	1.1358 ± 0.0004	1.348 ± 0.003	1.496 ± 0.003	1.637 ± 0.002	1.485 ± 0.008
$N = \infty$	1.37 ± 0.03	1.301 ± 0.006				

nodes at critical value cannot explain the observed power-law distributed avalanches on their own. There has to be another mechanism or another configuration of critical clusters, which we appear to have found.

We demonstrated that a simple split-and-merge operation of clusters of nodes in a network can explain the dependence of the exponent on the dimensionality of the space that the network is embedded in. In a higher-dimensional space, the magnitude of the exponent is larger, i.e., clusters tend to be smaller. Qualitatively, the same behavior has been observed in the BTW model [10].

Theoretically, analyzing our cluster-formation model, we found a direct relationship between the exponent of the cluster-size distribution and the ratio of the fractal dimension of the cluster boundary and the dimensionality of the embedding space. This relationship holds for sufficiently small ratios, $d_B/d < 0.9$. Based on the same relationship, we could approximately predict the exponent of the distribution of critical clusters in the 2D BTW model (1.247 vs 1.286) and in the Abelian sandpile model on a random geometric graph (1.27 vs 1.30). For the RGG, the difference between prediction and experiment was within the error bounds, but for the 2D lattice, there remained a systematic difference that was not explained by our statistical errors. This difference might arise from the uncertain extrapolation to infinite lattice size or the oversimplification of our cluster-formation process. In the BTW model, critical clusters may split into more than two parts or may form by combining more than two clusters.

The exponents of the critical clusters were close to those for the avalanche area distribution, but slightly different: in two to three dimensions, they were slightly smaller. The critical clusters are a subset of an avalanche area, and the percentage of this subset increases with increasing avalanche area (in lower dimensions), skewing the exponents to lower values.

Our predictions for the exponents of the BTW model do deviate from experimental results for higher-dimensional lattices. Based on the fractal dimensions, values above 1.5 would be expected, but the mean-field theory bounds these values to 1.5. So, we hypothesize that with increasing dimensionality, there is a transition between the cluster-formation process and the critical branching process [5] of the mean-field theory (Fig. 8). According to this hypothesis, a network embedded in an infinite dimensional space, e.g., an Erdős-Renyí network, will have an exponent of 1.5, which matches our experimental value for ER.

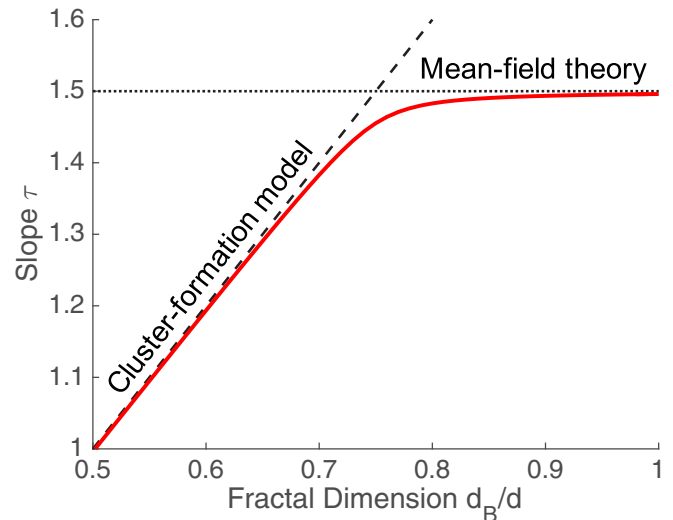


FIG. 8. Notional transition between cluster-formation dynamics and mean-field theory depending on the fractal dimension of clusters.

Our study provided insights into the mechanism of self-organized criticality. Particularly, it sheds light into the dependence on the network topology on top of which an SOC process is carried out. Moreover, we illustrated that likely no common mechanism exists that explains all phenomena attributed to SOC. Even within one model, the Abelian sandpile, we can, apparently, observe a transition between mechanisms when changing the network topology. Finding concrete mechanisms behind SOC phenomena will help us to strengthen the definition of SOC, understand where it occurs, and exploit it for application. More work is required to solidify if cluster formation is indeed the dominate process for BTW models in low dimensions and to which other SOC phenomena it applies.

ACKNOWLEDGMENTS

This material is based upon work supported by the Defense Advanced Research Projects Agency (DARPA) and Space and Naval Warfare Systems Center Pacific (SSC Pacific) under Contract No. N66001-15-C-4020. Any opinions, findings, and conclusions or recommendations expressed in this material are those of the author and do not necessarily reflect the views of DARPA or SSC Pacific.

- [1] P. Bak, C. Tang, and K. Wiesenfeld, *Phys. Rev. Lett.* **59**, 381 (1987).
- [2] J. M. Beggs and D. Plenz, *J. Neurosci.* **23**, 11167 (2003).
- [3] B. Gutenberg and C. F. Richter, *Bull. Seismol. Soc. Am.* **46**, 105 (1956).
- [4] H. Hoffmann and D. W. Payton, *Chaos Solitons Fractals* **67**, 87 (2014).
- [5] H. J. Jensen, *Self-Organized Criticality: Emergent Complex Behavior in Physical and Biological Systems*, Cambridge Lecture Notes in Physics (Cambridge University Press, Cambridge, UK, 1998).
- [6] Z. Olami, H. J. S. Feder, and K. Christensen, *Phys. Rev. Lett.* **68**, 1244 (1992).
- [7] K. Christensen and Z. Olami, *Phys. Rev. E* **48**, 3361 (1993).
- [8] S. A. Janowsky and C. A. Laberge, *J. Phys. A: Math. Gen.* **26**, L973 (1993).
- [9] S. Zapperi, K. B. Lauritsen, and H. E. Stanley, *Phys. Rev. Lett.* **75**, 4071 (1995).
- [10] A. Chessa, E. Marinari, A. Vespignani, and S. Zapperi, *Phys. Rev. E* **57**, R6241 (1998).
- [11] D. Dhar, *Phys. Rev. Lett.* **64**, 1613 (1990).
- [12] S. Lübeck and K. D. Usadel, *Phys. Rev. E* **55**, 4095 (1997).
- [13] J. L. Jacobsen, *J. Phys. A: Math. Theor.* **47**, 135001 (2014).